Inorganic Chemistry
Cite This: Inorg. Chem. 2018, 57, 13176−13187
Article
pubs.acs.org/IC

# Trapping of a Pseudotetrahedral $Co^{II}O_4$ Core in Mixed-Valence Mixed-Geometry [$Co_5$] Coordination Aggregates: Synthetic Marvel, Structures, and Magnetism

Krishna Chattopadhyay,[†,‡] María José Heras Ojea,[§] Arup Sarkar,[∥] Mark Murrie,*[,§] Gopalan Rajaraman,*[,∥] and Debashis Ray*[,†]

[†]Department of Chemistry, Indian Institute of Technology Kharagpur, Kharagpur 721 302, India
[‡]School of Chemical Sciences, Indian Association for the Cultivation of Science, Jadavpur, Kolkata 700032, India
[§]WestCHEM, School of Chemistry, University of Glasgow, University Avenue, Glasgow G12 8QQ, U.K.
[∥]Department of Chemistry, Indian Institute of Technology Bombay, Mumbai 400 076, India

Supporting Information

**ABSTRACT:** A systematic one-step one-pot multicomponent reaction of $Co(ClO_4)_2·6H_2O$, $H_3L$ (2,6-bis((2-(2-hydroxyethylamino)ethylimino)methyl)-4-methylphenol), and readily available carboxylate salts ($RCO_2Na$; R = $CH_3$, $C_2H_5$) resulted in the two structurally novel coordination aggregates $[Co^{II}Co^{III}_4L_2(\mu_{1,3}\text{-}O_2CCH_3)_2(\mu\text{-}OH)_2](ClO_4)_4·4H_2O$ (**1**) and $[Co^{II}Co^{III}_4L_2(\mu_{1,3}\text{-}O_2CC_2H_5)_2(\mu\text{-}OH)(\mu\text{-}OMe)](ClO_4)_4·5H_2O$ (**2**). At room temperature, reactions of $H_3L$ in MeOH with cobalt(II) perchlorate salts led to coassembly of initially formed ligand-bound $\{Co^{II}_2\}$ fragments following aerial oxidation of metal centers and bridging by in situ generated hydroxido/alkoxido groups and added carboxylate anions. Available alkoxido arms of the initially formed $\{L(\mu_{1,3}\text{-}O_2CCH_3)(\mu\text{-}OH/OMe)Co_2\}^+$ fragments were utilized to trap a central $Co^{II}$ ion during the formation of [$Co_5$] aggregates. In the solid state, both complexes have been characterized by X-ray crystallography, variable-temperature magnetic measurements, and theoretical studies. Both **1** and **2** show field-induced slow magnetic relaxation that arises from the single pseudo-$T_d$ $Co^{II}$ ion present. The structural distortion leads to an easy-axis magnetic anisotropy ($D$ = −31.31 $cm^{-1}$ for **1** and −21.88 $cm^{-1}$ for **2**) and a small but non-negligible transverse component ($E/D$ = 0.11 for **1** and 0.08 for **2**). The theoretical studies also reveal how the O−Co−O bond angles and the interplanar angles control $D$ and $E$ values in **1** and **2**. The presence of two diamagnetic $\{Co_2(\mu\text{-}L)\}$ hosts controls the distortion of the central $\{CoO_4\}$ unit, highlighting a strategy to control single-ion magnetic anisotropy by trapping single ions within a diamagnetic coordination environment.

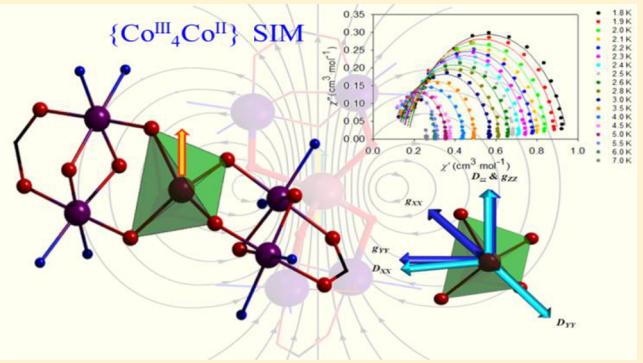


## INTRODUCTION

In recent years, the involvement of the organic phenoxido group as a primary coordinating site and the design of reaction protocols using these ligands for 'multicomponent self-aggregation' reactions of initially formed fragments have attracted enormous interest for the generation of multimetallic coordination complexes.[1−3] Attempts have therefore been made in the standardization of new synthetic strategies using phenol-centered binucleating ligands, leading to the formation of primary ligand and ancillary bridge clipped reaction products containing more than two metal ions. Thus, the choice of primary ligand and availability of ancillary clips were crucial in assembling the self-condensing precursors through simultaneous involvement of ligands/bridges and ligand side arms. Coordination capping by the primary ligand over several 3d metal ions can result in new structure types showing unique binding modes and promise for single-molecule magnets (SMMs)[4−6] and magnetic refrigerants.[7−9] Thus, room-temperature synthesis in high yield and characterization of such coordination aggregates have received renewed attention following the discovery of SMMs. Solubility in common organic solvents and reproducibility during synthesis are also important for this family of complexes to follow the path of aggregation and solution activity and behavior. Single-molecule magnets are exchange-coupled polymetallic complexes that possess a large ground-state spin ($S$) and sizable magnetic anisotropy ($D$), of importance in the modulation of the size of the barrier for reversal of magnetization, $U_{eff}$. Another family of molecular magnets based on single paramagnetic 3d and/or 4f ions in a suitable ligand field, known as single-ion magnets (SIMs), have shown promise in recent years.[10−15] The SMM

Received: June 7, 2018
Published: October 16, 2018






DOI: 10.1021/acs.inorgchem.8b01577
Inorg. Chem. 2018, 57, 13176−13187

behavior in the second category having a single transition-metal ion often depends on an unusual coordination geometry to generate a magnetically anisotropic ground state. One important strategy for obtaining SMM behavior follows from the observation that low-coordinate, high-spin iron(II) and cobalt(II) complexes can record large and negative $D$ values. Recently a cobalt(II) ion in $D_3$ symmetry, surrounded by diamagnetic cobalt(III) ions in a molecular agglomerate, has shown interesting SIM behavior.[16] The phenol-centered bis-diimine ligand ($H_nL$) family is known to give $\{M_2L\}^{n+}$ (M = 3d metal ions) species and has potential for self-aggregation in the presence of in situ generated $HO^-/RO^-$ ions and externally added $RCO_2^-$ ions.[17] In the recent past we reported the aggregation of $\{Co_2L\}^{n+}$ fragments around two in situ generated $CO_3^{2-}$ ions for a $[Co_5]$ wheel structure.[18]

While trying to synthesize a new family of cobalt ion based coordination aggregates from the self-assembly of ligand-bound $\{Co_2L\}^{n+}$ units, we have been interested in discovering the reactivity patterns of 2,6-bis((2-(2-hydroxyethylamino)-ethylimino)methyl)-4-methylphenol ($H_3L$; Chart 1, left) with

**Chart 1. Ligand and Its Metal Ion Binding Mode**

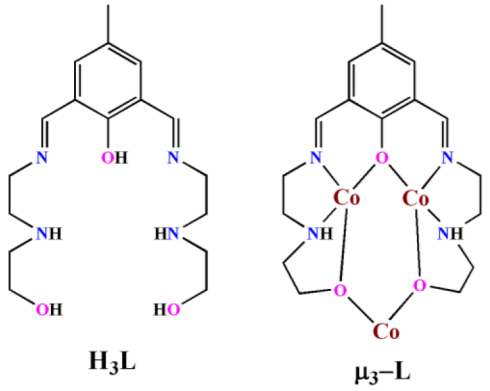


$Co(ClO_4)_2{\cdot}6H_2O$ in the presence of two different carboxylate salts ($RCO_2^-$, R = $CH_3$, $C_2H_5$). In the absence of any added base and in the presence of $RCO_2^-$, $H_3L$ in the trinegative form $L^{3-}$ binds three cobalt ions per unit in a $\mu_3$ mode (Chart 1, right). Previously, $H_3L$ resulted in $[Cu_6]$[19] and $[Ni_4]$, $[Ni_2]_n$ complexes,[20] where the alcohol side arms remained dangling without showing any metal ion coordination. If these side arms could engage in bridging coordination to other metal ion centers, it is reasonable to imagine other kinds of self-aggregation reactions based on $\{Co_2L\}^{n+}$ units. In addition to filling the vacant coordination positions around the metal centers, the externally added or metal salt derived carboxylates also modulate the pH of the reaction medium, which in turn controls the entrapment of $HO^-$ and $RO^-$ groups in the final structures.

Herein we present the results of our room-temperature synthetic investigations of the air- and moisture-stable mixed-valent mixed-geometry $[Co_5]$ aggregates $[Co^{II}Co^{III}{}_4L_2(\mu_{1,3}\text{-}O_2CCH_3)_2(\mu\text{-}OH)_2](ClO_4)_4{\cdot}4H_2O$ (**1**) and $[Co^{II}Co^{III}{}_4L_2(\mu_{1,3}\text{-}O_2CC_2H_5)_2(\mu\text{-}OH)(\mu\text{-}OMe)](ClO_4)_4{\cdot}5H_2O$ (**2**), where $H_3L$ is 2,6-bis((2-(2-hydroxyethylamino)-ethylimino)methyl)-4-methylphenol. We were unable to isolate the cationic $[Co_2]$ complex from the reaction medium due to triggering of the facile and spontaneous in situ self-aggregation reactions. The standardized synthesis, growth of crystals, molecular structures, and magnetic properties of these complexes are described and discussed.

## EXPERIMENTAL SECTION

**Materials.** Hydrated cobalt(II) perchlorate salt was prepared by treating cobalt(II) carbonate with a 1:1 aqueous solution of concentrated perchloric acid. Other chemicals used in this work were *N*-(hydroxyethyl)ethylenediamine and sodium acetate obtained from Alfa Aesar and cobalt(II) carbonate from SD Fine-Chem Ltd., India. Sodium propionate was prepared by treating propionic acid (11.1 g, 0.15 mol) with solid sodium hydroxide (6.0 g, 0.15 mol), followed by concentration and crystallization on a water bath. 2,6-Diformyl-4-methylphenol (dialdehyde) was prepared following a literature procedure with some modifications.[21] All other chemical compounds and solvents were reagent-grade materials and were used as received without further purification.

*Caution!* Although we did not face any problem during the synthesis of the reported compounds, metal ion complexes of organic ligands having perchlorate ions as counteranions are known to be potentially explosive in nature. Only a small amount of the material was prepared at a time and was handled with utmost care.

**Synthetic Protocol.** *Ligand Synthesis: 2,6-Bis{(2-(2-hydroxyethylamino)ethylimino)methyl}-4-methylphenol ($H_3L$).* The ligand $H_3L$ was synthesized following our previously reported work.[19]

*Complex Synthesis.* A general synthetic procedure was followed for the synthesis of **1** and **2** in good yield from the reactions of $Co(ClO_4)_2{\cdot}6H_2O$ and $H_3L$ in the presence of sodium acetate and sodium propionate, respectively.

A MeOH (10 mL) solution of $Co(ClO_4)_2{\cdot}6H_2O$ (0.91 g, 2.5 mmol) was added dropwise over 10 min to an orange MeOH (10 mL) solution of $H_3L$ (0.34 g, 1.0 mmol) at room temperature with continuous stirring. After 10 min, the brown solution became colloidal and it was treated with a MeOH solution of $RCO_2Na$ (2 mmol; R = $-CH_3$, $-C_2H_5$), during which the reaction mixture turned brown. The mixture was stirred for 30 min at room temperature and then refluxed for another 1 h. After it was cooled to room temperature, the solution was filtered through a G4 sintered bed and slow evaporation of the solvent from the filtrate provided brown block-shaped crystals suitable for X-ray analysis after 15−20 days.

*$[Co^{II}Co^{III}{}_4L_2(\mu_{1,3}\text{-}O_2CCH_3)_2(\mu\text{-}OH)_2](ClO_4)_4{\cdot}4H_2O$ (**1**).* Sodium acetate was used as the source of carboxylate anion for synthesis of **1**. Yield: 0.36 g, 45%. Anal. Calcd for $C_{38}H_{64}Cl_4Co_5N_8O_{32}$ (1583.38 g $mol^{-1}$): C, 28.86; H, 4.08; N, 7.09. Found: C, 29.19; H, 4.01; N, 6.98. Selected FTIR peaks (KBr, $cm^{-1}$; s = strong, vs = very strong, m = medium, br = broad): 3421 (br), 1654 (s), 1571 (s), 1437 (m), 1139 (m), 1089 (vs), 626 (s). Molar conductance, $\Lambda_M$ (MeCN solution, $\Omega^{-1}$ $cm^2$ $mol^{-1}$): 242.5. UV−vis spectra ($\lambda_{max}$, nm ($\varepsilon$, L $mol^{-1}$ $cm^{-1}$)) (MeCN solution): 617 (501), 385 (59000).

*$[Co^{II}Co^{III}{}_4L_2(\mu_{1,3}\text{-}O_2CC_2H_5)_2(\mu\text{-}OH)(\mu\text{-}OMe)](ClO_4)_4{\cdot}5H_2O$ (**2**).* Sodium propionate was used in lieu of sodium acetate for the synthesis of **2**. Yield: 0.34 g, 42%. Anal. Calcd for $C_{41}H_{74}Cl_4Co_5N_8O_{33}$ (1640.43 g $mol^{-1}$): C, 29.96; H, 4.54; N, 6.82. Found: C, 30.07; H, 4.51; N, 6.76. Selected FTIR peaks (KBr, $cm^{-1}$; s = strong, vs = very strong, m = medium, br = broad): 3421 (br), 1654 (s), 1571 (s), 1458 (m), 1143 (m), 1114 (m), 1086 (vs), 627 (s). Molar conductance, $\Lambda_M$ (MeCN solution, $\Omega^{-1}$ $cm^2$ $mol^{-1}$): 260.4. UV−vis spectra ($\lambda_{max}$, nm ($\varepsilon$, L $mol^{-1}$ $cm^{-1}$)) (MeCN solution): 617 (561), 364 (14129).

**Physical Measurements.** Elemental analysis of the compounds was performed with a PerkinElmer (model 240C) elemental analyzer for C, H, and N contents. A Shimadzu UV 3100 UV−vis−NIR spectrophotometer was used for electronic spectral data collection, and a PerkinElmer RX1 spectrometer was used to record the FT-IR spectra. Powder X-ray diffraction (PXRD) patterns were measured on a Bruker AXS X-ray diffractometer (40 kV, 20 mA) using Cu K$\alpha$ radiation ($\lambda$ = 1.5418 Å) within the 5−50° ($2\theta$) range and a fixed-time counting of 4 s at 25 °C.



DOI: 10.1021/acs.inorgchem.8b01577
*Inorg. Chem.* 2018, 57, 13176−13187

**Scheme 1. Preferred Synthetic Routes for 1 and 2**

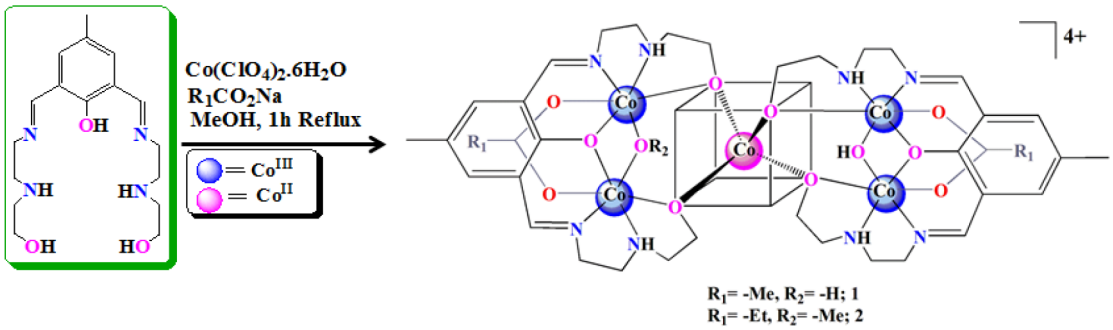


**Magnetic Measurements.** Direct current (dc) and alternating current (ac) magnetic measurements for the two complexes **1** and **2** were carried out using polycrystalline samples constrained in eicosane, using a Quantum Design SQUID magnetometer equipped with a 5 T magnet at the School of Chemistry at the University of Glasgow. The dc measurements were performed in the temperature range 290−2 K under an applied field of 1000 Oe. Field-dependent magnetization measurements were performed at 2, 4, and 6 K, over the range 0−5 T. Dynamic susceptibility measurements were performed over the temperature range of 2−10 K, with a drive field of 3 Oe and a frequency range from 1 to 1488 Hz. Data were corrected for the diamagnetic contribution of the sample holder and eicosane by measurements and for the diamagnetism of the compounds.

**Computational Details.** All of the first-principles calculations have been performed using the ORCA 4.0.0 program package on the X-ray strctures.[22] We have employed the def2-TZVP basis set on Co, the def2-TZVP(-f) basis set for N and O and the def2-SVP basis set for the rest of the atoms.[23−26] With these basis sets, state averaged complete active space self-consistent field (SA-CASSCF) calculations were performed on **1** and **2**. The active space in this calculation is comprised of seven d electrons of Co in five d orbitals i.e., CAS(7,5). Using this active space, we have computed 10 quartet and 40 doublet roots in the CI (configuration interaction) step. To incorporate the dynamic correlation, we have employed *N*-electron valence perturbation theory (NEVPT2) on top of the CASSCF wave function. To account for the scalar relativistic effects, the zeroth-order regular approximation (ZORA) method was used in the Hamiltonian as well as in the basis functions during all of the calculations. The zero-field splitting parameters (*D* and *E*) were calculated from both second-order perturbation theory and the modern effective Hamiltonian approach (EHA).[25] The spin−orbit coupling effects were incorporated by using a quasi-degenerate perturbation theory (QDPT) approach.

Separately single-point DFT calculations were performed in the Gaussian 09 (revision A.02) program package.[26] For this, the unrestricted-B3LYP (UB3LYP) hybrid functional on both the complexes with all-electron triple-ζ valence (TZV) basis set was used.

**X-ray Crystallography.** Appropriate single crystals of **1** and **2** were chosen for X-ray diffraction. The data were collected using a Bruker SMART APEX-II CCD X-ray diffractometer, equipped with a graphite monochromator. Mo Kα radiation (λ = 0.71073 Å) was used as the X-ray source. The experiments were performed by the ω-scan method at 293 K with 4 s counting time per frame. The space groups were determined by XPREP,[27] and the data processing was performed with the SAINT software. The structures were solved by employing direct methods using the SHELXS-97 program[28] and refined with full-matrix least squares on $F^2$ using the SHELXL-2014[29] program package associated with the WINGX system, version 1.80.05.[30] Multiscan empirical absorption corrections were applied to the data using the program SADABS.[31] The locations of the heaviest atoms (Co) were determined easily. The positions of O, N, and C atoms were determined from the difference Fourier maps. These atoms were refined anisotropically. The H atoms were introduced in calculated positions and refined with fixed geometry and riding thermal parameters with respect to their carrier atoms. Crystallographic diagrams were generated using DIAMOND[32] and POV-ray software.[33] The information regarding the X-ray data collection and structure refinement of compounds **1** and **2** is summarized in Table S1. CCDC 1534950 and 1534949 contain the supplementary crystallographic data for **1** and **2**.

## RESULTS AND DISCUSSION

**Single-Step Aggregation Reaction.** In MeOH the Schiff base condensation reaction of 2,6-diformyl-4-methylphenol and *N*-(hydroxyethyl)ethylenediamine in a 1:2 molar ratio resulted in $H_3L$.[16] Reactions of $H_3L$ with $Co(ClO_4)_2·6H_2O$ were examined in the presence of externally added $RCO_2Na$ (R = $-CH_3$, $-C_2H_5$) salts in MeOH. Use of $H_3L$, $Co(ClO_4)_2·6H_2O$, and $CH_3CO_2Na$ in a 1:2.5:3 molar ratio followed by reflux resulted in a bright brown solution which provided **1** as brown block-shaped crystals in 45% yield (Scheme 1 and eq 1). Several other molar ratios for the reactants were examined in other solvent media and bases, before the reported ratio was established with good reproducibility. Changes in ratios and sequence of addition did not result in any other form of complex. The two hydroxido bridges, generated from the water molecules present in the reaction medium, were utilized for clipping the two parent ligand bound adjacent $Co^{III}$ centers in **1** (eq 1).

$$2H_3L + 5Co(ClO_4)_2·6H_2O + 6CH_3CO_2Na + O_2 \rightarrow [Co_5L_2(\mu_{1,3}\text{-}O_2CCH_3)_2(\mu\text{-}OH)_2](ClO_4)_4·4H_2O + 6NaClO_4 + 4CH_3CO_2H + 26H_2O \quad (1)$$

The coordination environment around the metal ions and the ligand field created by the ligand donors and ancillary groups favor the oxidation of four $Co^{II}$ centers to $Co^{III}$ by $O_2$ of air. Use of $CH_3CO_2Na$ salt from the outside serves a dual role, by providing intermetal ion bridges and in situ generation of $HO^-$ ions from water present in the reaction medium. Other bases such as $NEt_3$ and NaOMe were unsuccessful in the attempted reactions and did not yield any isolable solid product. Use of $C_2H_5CO_2Na$ in lieu of $CH_3CO_2Na$ resulted in a brown solution after 30 min of stirring of the reactants at room temperature followed by 1 h of reflux in MeOH. Slow evaporation of the solvent from the resulting solution produced **2** as brown block-shaped crystals in 42% yield. Formation of **2** can be summarized in eq 2, accounting for the generation of the required $HO^-$ and $MeO^-$ bridges from $H_2O$ and MeOH in the reaction medium.



DOI: 10.1021/acs.inorgchem.8b01577
Inorg. Chem. 2018, 57, 13176−13187

$$2H_3L + 5Co(ClO_4)_2\cdot 6H_2O + 6C_2H_5CO_2Na + O_2 + MeOH \rightarrow [Co_5L_2(\mu_{1,3}\text{-}O_2CC_2H_5)_2(\mu\text{-}OH)(\mu\text{-}OMe)](ClO_4)_4\cdot 4H_2O + 6NaClO_4 + 4C_2H_5CO_2H + 27H_2O \quad (2)$$

During the aggregation of **1** and **2** in solution, phenoxido coordination from deprotonated $H_3L$ together with water- and methanol-derived − -OH/−OMe bridges provide $[Co^{III}L(\mu\text{-}RCO_2)(\mu\text{-}OH/OMe)]^+$ fragments. Two such units next trap the available $Co^{2+}$ ion in solution by terminal alkoxido bridges of the parent ligands. Creation of a tetrahedral $\{O_4\}$ pocket by two $[Co^{III}L(\mu\text{-}RCO_2)(\mu\text{-}OH/OMe)]^+$ units and trapping of a single paramagnetic $Co^{II}$ center by them is comparatively rare in the literature from a synthetic point of view.[34,35]

**FTIR Characterization.** An analysis of bond stretching frequencies confirmed the stability of the complexes in the solid state and binding of two deprotonated ligands to five cobalt centers augmented by carboxylate capping. The characteristic $\bar{\nu}_{C=N}$ stretching frequencies for the metal ion bound ligand fragments appear at 1654 $cm^{-1}$. The presence of bridging $HO^-$ groups and lattice water molecules in **1** and **2** are detected as a single broad band in each case at 3421 $cm^{-1}$, assigned to a $\bar{\nu}_{OH}$ stretching frequency (Figure S1 in the Supporting Information). The presence of several $ClO_4^-$ anions for charge neutralization of cationic complexes was first diagnosed by FTIR bands in $T_d$ symmetry at 1089 and 1086 $cm^{-1}$ and medium bands at 626 and 627 $cm^{-1}$, due to the $\nu_3(T_2)$ ($\nu_{ClO}$) and $\nu_4(T_2)$ ($\delta_{dOClO}$) modes, respectively.[36] For complex **1**, asymmetric ($\bar{\nu}_{as}(COO)$) and symmetric ($\bar{\nu}_s(COO)$) stretching vibrations of the acetate groups are detected at 1571 and 1437 $cm^{-1}$, respectively. These peaks for the propionate group in **2** appear at 1571 and 1458 $cm^{-1}$. The $\Delta\nu$ ($\Delta\nu = \bar{\nu}_{as}(COO) - \bar{\nu}_s(COO)$) values of 134 and 113 $cm^{-1}$ did confirm the $\mu$-1,3 bridging modes of the carboxylates in **1** and **2**.[37]

**Powder X-ray Diffraction Patterns.** The purity of the complexes was assessed from their powder X-ray diffraction patterns using as-synthesized bulk powder materials for **1** and **2**. The obtained patterns are in good agreement with the simulated patterns obtained from the single-crystal X-ray diffraction data using Mercury software. Figure S2 in the Supporting Information displays the correlation between the experimental and simulated patterns, which confirms that the bulk materials have the same phase purity as that of the single crystals.

**Electronic Spectra.** The characteristic electronic structural patterns were identified by measuring their solution electronic spectra. In MeCN solutions, **1** and **2** display a number of bands in the 600−200 nm range (Figure S3 in the Supporting Information). The absorption bands in the visible region with maxima ($\lambda_{max}$) at 557 nm ($\varepsilon$ = 643 L $mol^{-1}$ $cm^{-1}$) and 555 nm ($\varepsilon$ = 770 L $mol^{-1}$ $cm^{-1}$) for **1** and **2**, respectively, can be assigned to spin-allowed $^4A_2 \rightarrow {}^4T_1$ (P) transitions originating from a $Co^{II}$ ion within distorted $O_4$ tetrahedral environments.[38,39] The lower energy shoulder peaks at 597 nm ($\varepsilon$ = 510 L $mol^{-1}$ $cm^{-1}$) and 616 nm ($\varepsilon$ = 501 L $mol^{-1}$ $cm^{-1}$) for **1** and 596 nm ($\varepsilon$ = 610 L $mol^{-1}$ $cm^{-1}$) and 617 nm ($\varepsilon$ = 501 L $mol^{-1}$ $cm^{-1}$) for **2** originates from the possible spin−orbit coupling of the $^4A_2 \rightarrow {}^4T_1$ (P) absorption envelope in the presence of a low symmetry ligand field.[40,41] This fact suggests that the $Co^{II}$ centers are in a slightly distorted tetrahedral geometry. The four ligand-bound low-spin $Co^{III}$ centers, on the other hand, did not contribute anything for d−d transitions but showed phenoxido → $Co^{III}$ LMCT transitions at 383 nm ($\varepsilon$ = 4800 L $mol^{-1}$ $cm^{-1}$) and 385 nm ($\varepsilon$ = 5400 L $mol^{-1}$ $cm^{-1}$) for **1** and **2**, respectively.[42] The intense and high-energy absorptions below 250 nm were attributed to intraligand $\pi \rightarrow \pi^*$ LLCT transitions centered on C═C and C═N backbones of $Co^{III}$- and $Co^{II}$-bound anionic ligands.

**Description of Crystal Structures.** Evaporation of solvent from MeOH solutions of **1** and **2** gave single crystals of suitable quality for X-ray structure determination.

*$[Co^{II}Co^{III}_4L_2(\mu\text{-}OH)_2(\mu_{1,3}\text{-}O_2CCH_3)_2](ClO_4)_4\cdot 4H_2O$ (**1**).* The molecular structure of the mixed-valence cationic complex unit $[Co_5L_2(\mu\text{-}OH)_2(\mu\text{-}O_2CCH_3)_2]^{4+}$ in **1** is shown in Figure 1, and important bond distances and angles are provided in Table S2 in the Supporting Information. Complex **1** crystallizes in the triclinic space group $P\bar{1}$. The structure consists of the pentanuclear fragment $[Co_5L_2(\mu\text{-}OH)_2(\mu_{1,3}\text{-}O_2CC_2H_5)_2]^{4+}$, four perchlorate anions, and four lattice water molecules.

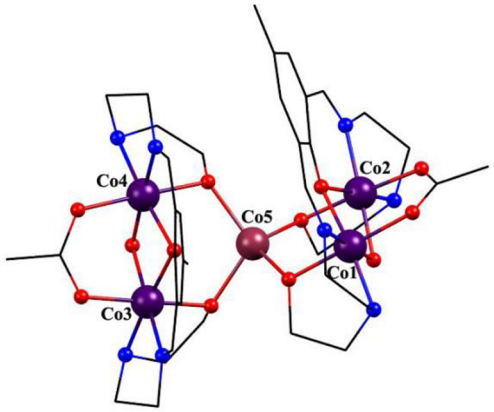


**Figure 1.** POV-ray presentation of the complex cationic unit in **1** with partial atom-numbering scheme. Counteranions, H atoms, and solvents of crystallization are omitted for clarity. Color code: C, black; N, blue; O, red; Co(III), violet, Co(II), pink.

A novel mixed-valence $[Co_5]$ core has been established from the use of the structure-directing diamine alcohol arms, imine backbone, and phenoxido bridges from the ligand $H_3L$. The pentanuclear complex units consist of two fully deprotonated ligand units ($L^{3-}$), each of them delivering two adjacent $N_2O_2$ donor sets to trap two $Co^{III}$ centers. Within the ligand ($L^{3-}$)-bound, phenoxido-hydroxido-bridged $\{Co_2L(OH)\}$ fragments, the $Co^{III}\cdots Co^{III}$ separations are in the range 2.806−2.810 Å (Table S2 in the Supporting Information). The growth of the structure of **1** may be presumed to occur through spontaneous aggregation of two $\{Co_2(\mu\text{-}L)(\mu\text{-}OH)\}$ units around the central $Co^{II}$ ion. Formation of these fragments was triggered by in situ generation and utilization of $HO^-$ ions. Carboxylate capping ligands were important in bringing the triply bridged $\{Co_2(\mu\text{-}L)(\mu\text{-}OH)(\mu\text{-}O_2CCH_3)\}$ motifs in a suitable distance to trap the $Co^{II}$ ion in a pseudotetrahedral geometry, without intervention of any other auxiliary coordinating/bridging ligand. The meridional fold of the imine-amine-alcohol arms of the parent ligand was crucial for appropriate disposition of the four oxygen atoms to bind the central $Co^{II}$ ion in a tetrahedral coordination geometry. All of the adjacent $Co^{III}$ centers (Co1, Co2, Co3, and Co4) remain in tetragonally distorted $N_2O_4$ octahedral coordination environments (Figure 2). The Co−N distances are different at 1.882(7) and 1.938(7) Å, respectively, for imine and amine coordination.


DOI: 10.1021/acs.inorgchem.8b01577
Inorg. Chem. 2018, 57, 13176−13187

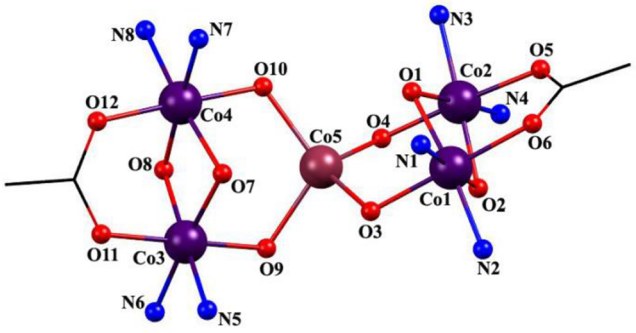


**Figure 2.** Core view of **1**. Color code: C, black; N, blue; O, red; Co(III), violet, Co(II), pink.

The endogenous phenoxido bridges from the ligands adjust the Co−O−Co angles to 94.4(2)−94.9(2)°, while the exogenous $HO^-$ bridges have Co−O−Co angles in the 95.6(2)−95.7(3)° range. The bridging alkoxido donors from meridionally folded imine-amine-alcohol arms asymmetrically bridge between octahedral $Co^{III}$ and tetrahedral $Co^{II}$ centers. Thus, Co−O distances were shorter (1.870−1.939 Å) at the octahedral sites for smaller $Co^{III}$ ions in comparison to tetrahedral (Co−O distances 1.969−2.008 Å) $Co^{II}$ ions.[43] Interestingly the short $C_2$ spacer bearing imine-amine-alcohol arms were meridionally ligated to the octahedral $Co^{III}$ ions, which is quite uncommon during chelate formation from chelating side arms of $L^{3-}$.

The O−Co−O angles around the central $Co^{II}$ ion range from 134.2(2) to 92.8(2)°. The Houser geometry index $\tau_4$ ($\tau_4$ = [360° − ($\alpha$ + $\beta$)]/141°; $\alpha$ and $\beta$ being the two largest angles) for the central $Co^{II}$ ion is 0.78, confirming a slightly flattened tetrahedral geometry.[44] The $\tau_4$ value is 1.00 for a perfect tetrahedral environment and 0.00 for a truly square planar geometry. The geometry assignment is again verified by symmetry analyses performed with SHAPE[45] (vide infra in Magnetic Properties). The assignment of +3 and +2 oxidation states to octahedral and tetrahedral cobalt ion centers, respectively, were evident from the bond distances and were further confirmed by BVS analysis (Table S3 in the Supporting Information).[46,47] Four lattice water molecules and four perchlorate anions associated with the [$Co_5$] aggregate were responsible for an intricate hydrogen-bonding network. Further, coordinated amine −NH donors of the ligands (D) and bridging hydroxido groups (D) were also involved in hydrogen-bonding interactions with perchlorate counteranions (A) and the lattice water molecules (A). This network connectivity in **1** results in a hydrogen-bonded dimeric assembly of two [$Co_5$] units, as shown in Figure 3. The D···A separations range within 2.17−3.217 Å while the D−H···A angles fall in a wide range spanning 112−162° (Table S4 in the Supporting Information).

*$[Co^{II}Co^{III}_4L_2(\mu_{1,3}\text{-}O_2CC_2H_5)_2(\mu\text{-}OH)(\mu\text{-}OMe)](ClO_4)_4\cdot 5H_2O$ (**2**).* Complex **2** crystallizes in the monoclinic space group $P2_1/c$, as illustrated in Figure 4. Aggregation of two dissimilar {$Co_2(\mu$-L)} units bridged by solvent-derived $HO^-$ and $MeO^-$ groups around the tetrahedral $Co^{II}$ ion generate **2**. The Co−O bond lengths at the $Co^{III}$ side from phenoxido, hydroxido, methoxido, and propionato coordination/bridging were in the range 1.880(7)−1.932(7) Å. All other metric parameters are like those for complex **1**.

Within the {$Co_2$L} fragment the $Co^{III}$···$Co^{III}$ separations were at 2.801(2)−2.805(2) Å. In this case the $MeO^-$ bridge

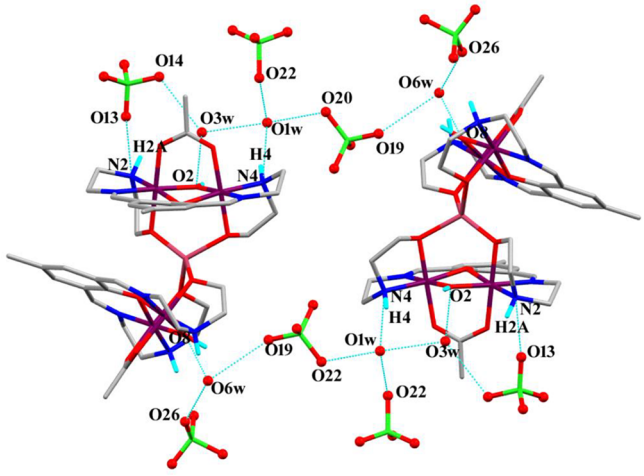


**Figure 3.** H-bonding network associated with **1**.

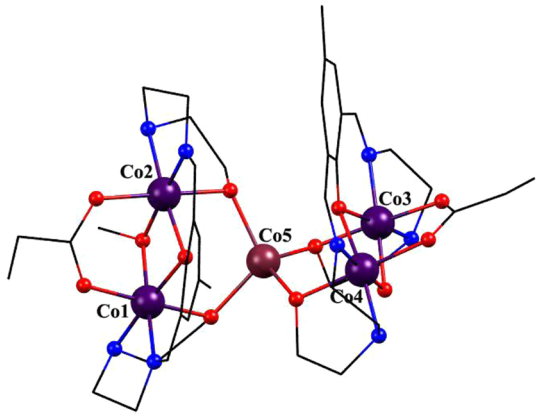


**Figure 4.** POV-ray presentation of the cationic part of **2** with partial atom-numbering scheme. Counteranions, H stoms, and solvents of crystallization are omitted for clarity. Color code: C, black; N, blue; O, red; Co(III), violet, Co(II), pink.

angle in Co−O−Co is 95.5(3)° and is slightly different from that of the $HO^-$-bridged part (96.1(3)°).The observed Co−O distances around the pseudotetrahedral $Co^{II}$ site span from 1.973(7) to 2.016(6) Å, and the O−Co−O angles extend from 96.1(3) to 129.9(3)°. The core structure of **2** (Figure S4 in the Supporting Information) shows the twisting arrangement of {$Co_2(\mu$-L)($\mu$-OH)($\mu$-$O_2CC_2H_5$)} and {$Co_2(\mu$-L)($\mu$-OMe)($\mu$-$O_2CC_2H_5$)} fragments around the central cobalt(II) ion. The $\tau_4$ value for **2** is 0.82, indicating a slightly smaller distortion from ideal tetrahedral geometry in comparison to that observed in **1**, which is confirmed from the CShMs obtained from the SHAPE symmetry analyses (vide infra).[44] Herein five lattice water molecules and four perchlorate anions are entangled in hydrogen-bonding interactions, leading to a H-bonded 1D chain involving lattice anions and solvent molecules (Figure S5 in the Supporting Information). The D···A distances vary from 3.012(15) to 3.29(2) Å while the D−H···A angles remain within 136.0−166.0°.

**Magnetic Properties.** The dc magnetic susceptibilities of both complexes were studied in an applied field of 1000 Oe in the temperature range of 290−2 K (see Figure S6 in the Supporting Information). Considering that octahedral LS-$Co^{III}$ ions are diamagnetic, the magnetic properties of the complexes are essentially defined by the central $Co^{II}$ ion. The


DOI: 10.1021/acs.inorgchem.8b01577
*Inorg. Chem.* 2018, 57, 13176−13187

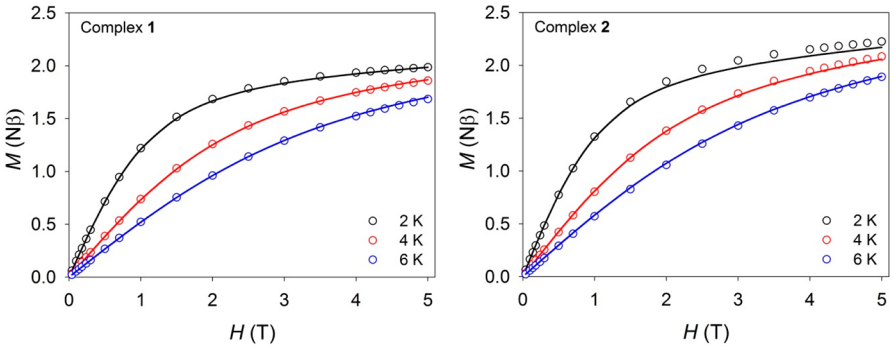


**Figure 5.** $M$ vs $H$ at 2, 4, and 6 K for **1** (left) and **2** (right). Fits are shown as solid lines (see text for details).

experimental values of $\chi_M T$ at room temperature for complex **1** (2.77 $cm^3$ $mol^{-1}$ K) and complex **2** (3.12 $cm^3$ $mol^{-1}$ K) are considerably higher than the expected value for an isotropic $S$ = 3/2 spin ($S$ = 3/2, $g$ = 2, 1.88 $cm^3$ $mol^{-1}$ K), indicating a spin−orbit coupling contribution. Below 290 K the $\chi_M T$ products gradually decrease with temperature until ∼50 K, and then a sharp drop is observed, reaching a minimum of 1.49 $cm^3$ $mol^{-1}$ K (**1**) and 1.62 $cm^3$ $mol^{-1}$ K (**2**) at 2 K. The displayed behavior indicates the presence of significant magnetic anisotropy from the $Co^{II}$ centers in both complexes. Variable-field magnetization experiments of **1** and **2** were also performed in the applied field range of $H$ = 0.4−5 T at different constant temperatures (2, 4, and 6 K). The plots (Figure 5) show that the magnetization does not reach saturation, in accord with the magnetic anisotropy suggested by the dc data. A simultaneous fit of the susceptibility and the magnetization data was carried out to investigate the parameters affected by magnetic anisotropy arising from crystal field effects ($g$, $D$).[48]

As $Co^{II}$ complexes can display positive or negative $D$ values, a survey of the data was performed (considering $-50 \geq D \geq 50$, $2.0 \geq g \geq 2.6$). The results from the survey suggest that there is not a unique solution, as multiple local minimum residuals were found for $D$. Hence, ab initio calculations were performed to give the zero-field splitting ($D$, $E$) and the $g$ parameters related to complexes **1** and **2** (see Table 1). The

**Table 1. Computed Spin Hamiltonian Parameters for Complexes 1 and 2**

| complex | methodology | $D$ ($cm^{-1}$) | $E/D$ | $g_X$ | $g_Y$ | $g_Z$ |
|---|---|---|---|---|---|---|
| **1** | CASSCF | −35.2 | 0.13 | 2.18 | 2.28 | 2.63 |
| | NEVPT2 | −31.3 | 0.11 | 2.14 | 2.22 | 2.54 |
| **2** | CASSCF | −25.1 | 0.10 | 2.20 | 2.26 | 2.52 |
| | NEVPT2 | −21.9 | 0.08 | 2.16 | 2.21 | 2.44 |

calculations propose orientation-dependent $g$ values ($g_x$, $g_y$, and $g_z$ from NEVPT2 being respectively 2.14, 2.22, and 2.54 for **1** and 2.16, 2.21, and 2.44 for **2**), relatively high and negative axial $D$ terms ($D$ = −31.31 $cm^{-1}$ for **1** and −21.88 $cm^{-1}$ for **2**) and a small but non-negligible transverse component ($E/D$ = 0.11 for **1** and 0.08 for **2**). Note that both axial anisotropic ZFS components ($D$) proposed are relatively large but are still reasonable for mononuclear pseudo-$T_d$ $Co^{II}$ complexes.[49−51] Consequently, fits for **1** and **2** were performed considering the calculated $D$ and $E/D$ components as fixed values and an average $g$ value as a variable parameter to avoid over-parameterization. A temperature-independent paramagnetism (TIP) term was also included as fixed parameter during the fit, given the presence of four $Co^{III}$ ions (TIP = 800 × $10^{-6}$ $cm^3$ $mol^{-1}$).[52] The best results (shown as solid lines in the $\chi_M T$ vs $T$ (Figure S6 in the Supporting Information) and $M$ vs $H$ (Figure 5) plots) give $g$ = 2.402 ± 0.002 (**1**) and 2.437 ± 0.008 (**2**), in reasonable agreement with those proposed from the ab initio calculations ($g \approx 2.3$). The small differences in the $g$ values between **1** and **2** could arise from subtle changes in the geometry around the Co(II) ions. Symmetry analyses performed with SHAPE[45] show that Co(II) in **2** is closer to the ideal $T_d$ geometry (CShMs = 1.818) than in **1** (2.558). This could also explain the difference in the calculated zero-field splitting terms for **1** and **2**.[53]

Considering the significantly large anisotropy suggested by the fit of the dc data, the magnetization dynamics of **1** and **2** were investigated. Ac susceptibility studies were performed as a function of temperature and/or frequency in zero applied dc field and in different dc fields. For both complexes in the absence of a dc field, no signal was observed in the out-of-phase susceptibility ($\chi''$) (Figures S7 and S8, left, in the Supporting Information). However, when a dc field is applied, an out-of-phase signal is observed (Figures S7 and S8, right). Isothermal field sweep ac susceptibility experiments as a function of frequency were then performed to find the optimum dc field for **1** and **2** (Figures S9 and S10 in the Supporting Information). The isothermal field sweep measurements for **1** suggest the presence of multiple field-dependent processes, as the Cole−Cole plots display a deviation at high field from the symmetric semicircles characteristic of a single relaxation process. As no maximum was observed in the $\tau$ vs $H$ data (see Figure S9), we performed the dynamic studies at 500 Oe. The dynamic studies at $H_{dc}$ = 500 Oe display a frequency-dependent out-of-phase signal (Figure 6). The Cole−Cole plots of the ac data between 1.8 and 7 K show a symmetrical shape for all of the temperatures (Figure 6, top right), and thus the Debye model for a single relaxation time was applied to fit the data. The $1/\tau$ vs $T$ plot (Figure 6, bottom right) shows temperature dependence above ∼4 K, which can be related to the presence of multiple processes. First attempts to fit $1/\tau$ vs $T$ data including the Orbach contribution (see Figure S11, left, in the Supporting Information) yield an energy barrier value ($(\Delta E/k_B)_1 \approx 50$ K) significantly lower than that calculated using the $D$ and $E$ values obtained from the ab initio study ($(\Delta E/k_B)_{cal} = 2\sqrt{(D^2 + 3E^2)} \approx 90$ K).[54] This can be ascribed to quantum tunneling of the magnetization, promoted by the rhombic term $E$ in previous studies on Co(II)-based SIMs or other possible spin-phonon relaxation mechanisms, as shown in Fe(II) SIMs.[55,56] However, the absence of a real state



DOI: 10.1021/acs.inorgchem.8b01577
Inorg. Chem. 2018, 57, 13176−13187

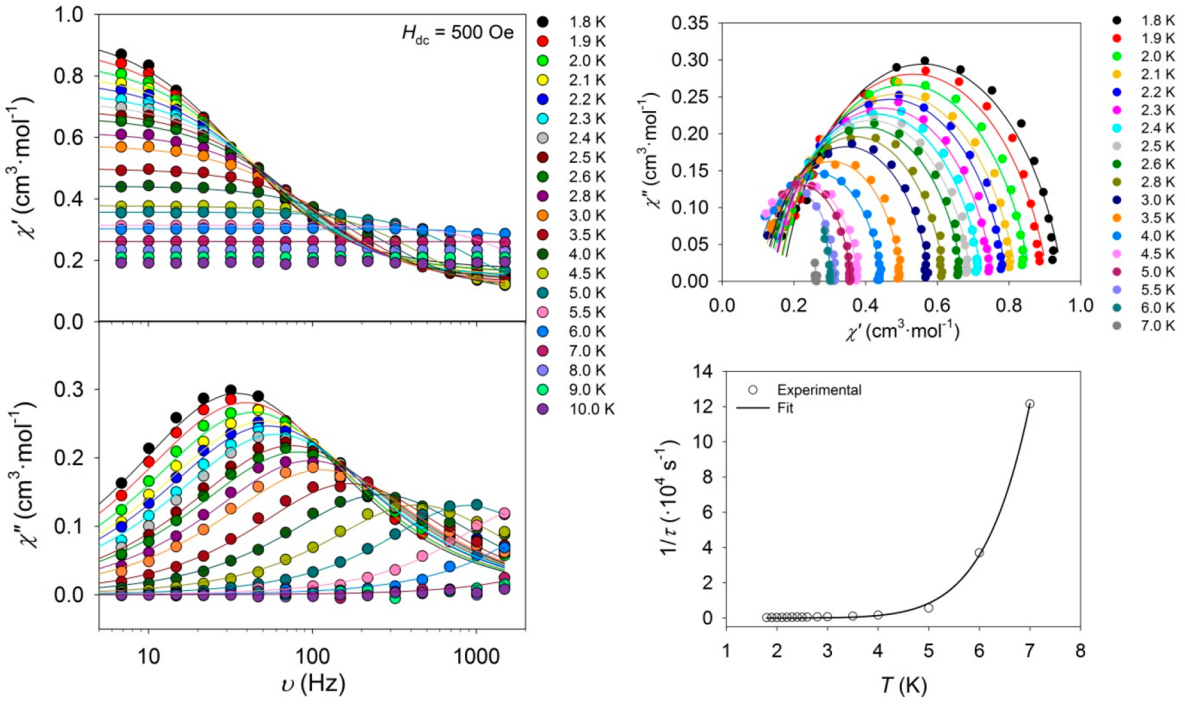


**Figure 6.** Dynamic magnetic properties for complex **1**: (left) ac magnetic susceptibility data at different frequencies in a dc field of 500 Oe; (right) Cole−Cole plots (top) and temperature dependence of the relaxation rate ($1/\tau$ vs $T$, bottom) from the $H_{dc}$ = 500 Oe data. The solid lines correspond to the fit (see text for details).

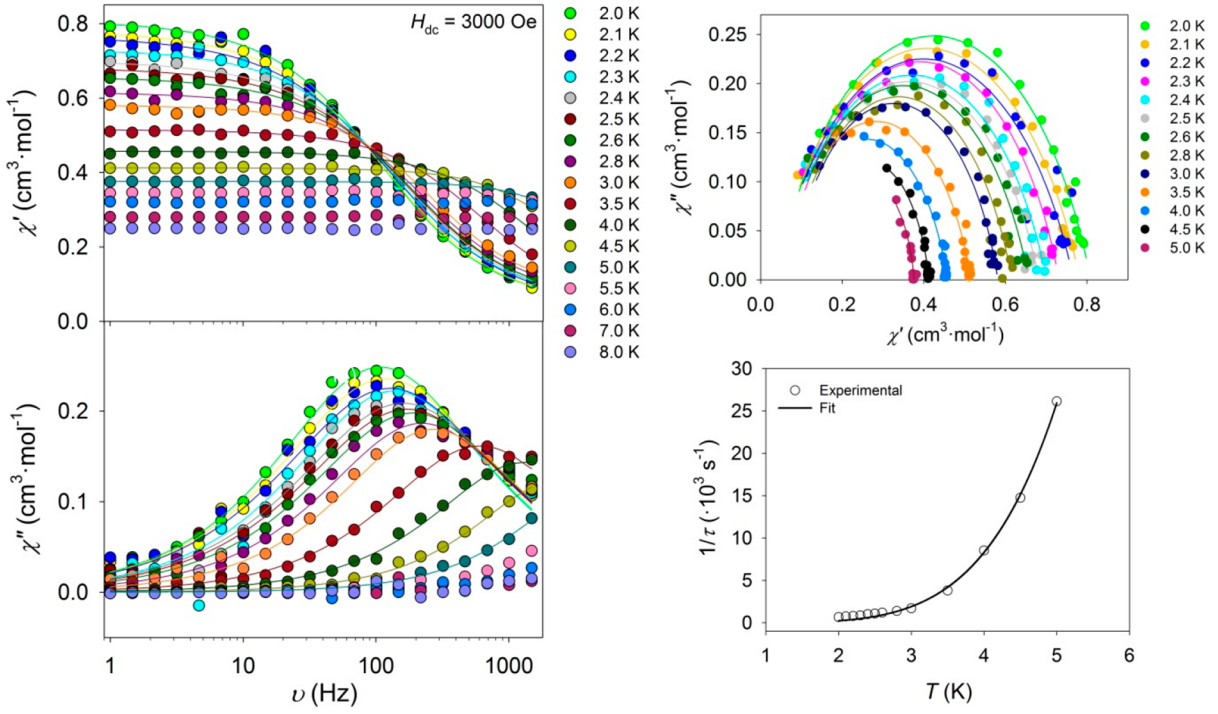


**Figure 7.** Dynamic magnetic properties for complex **2**: (left) ac magnetic susceptibility data at different frequencies in a dc field of 3000 Oe; (right) Cole−Cole plots (top) and temperature dependence of the relaxation rate ($1/\tau$ vs $T$, bottom) from the $H_{dc}$ = 3000 Oe data. The solid lines correspond to the fit (see text for details).

at the energy gap proposed by the fit suggests that the reversal of the magnetization should occur via relaxation processes alternative to Orbach.[57−59] Therefore, and in order to avoid overparameterization, the fit of the $1/\tau$ vs $T$ data at $H_{dc}$ = 500 Oe is performed considering only the Raman contribution (see eq 3).

$$\tau^{-1} = CT^{n} \quad (3)$$



DOI: 10.1021/acs.inorgchem.8b01577
*Inorg. Chem.* 2018, 57, 13176−13187

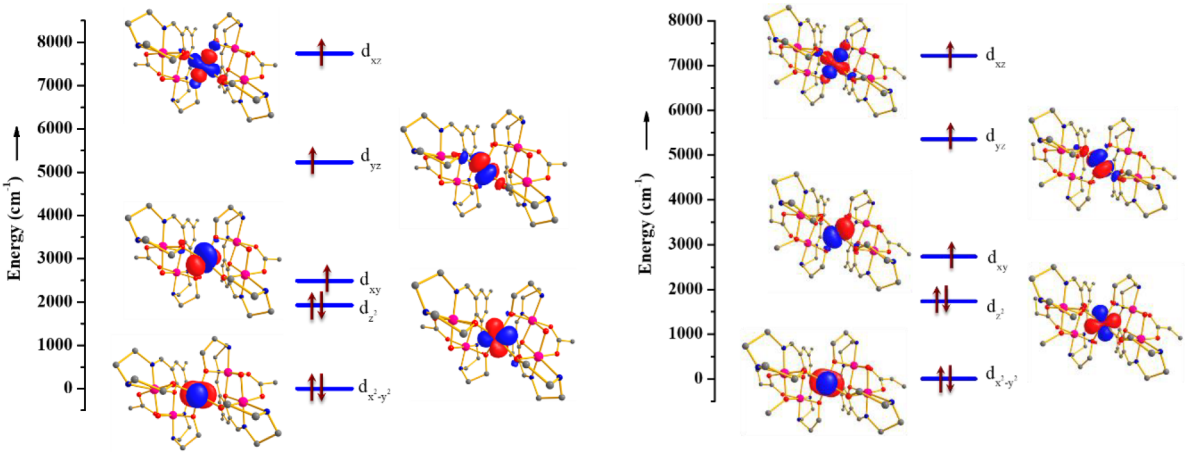


**Figure 8.** CASSCF-LFT orbital splitting diagrams of complex **1** (left) and complex **2** (right). Note here that the orbital labels reflect the major coefficient in the corresponding wave function.

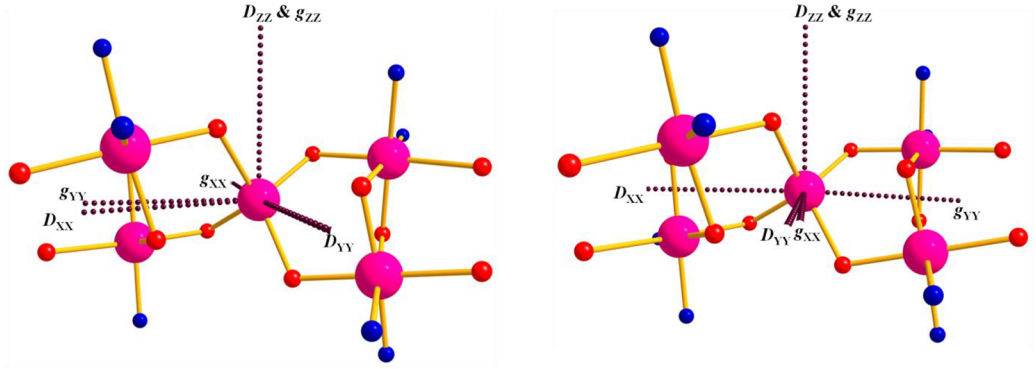


**Figure 9.** $D$ and $g$ anisotropy axes of complexes **1** (left) and **2** (right). $D_{ZZ}$ and $g_{ZZ}$ axes indicate the molecular $z$ direction. Color code: Co, pink; O, red; N, blue (C and H atoms are omitted for clarity).

Note that the slow relaxation is promoted by the application of a dc field, suggesting QTM. However, models for fitting the $1/\tau$ vs $T$ data (see Figure 6) and/or the field-dependent data (see data in Figure S9 in the Supporting Information) including the tunneling contribution did not reproduce the tendency displayed in the plots. The best results (shown as a solid black line in Figure 6 bottom right) are $C = 0.02$ s$^{-1}$ K$^n$, $n = 7.96$. Although $n = 9$ for a Kramers ion (or 5 in the presence of low-lying states),[14,60] the slightly lower estimated value ($n = 7.96$) may arise from the presence of both acoustic and optical phonons.[53,61,62]

In contrast to **1**, the field dependence of the relaxation time for **2** (Figure S10, bottom right, in the Supporting Information) clearly displays a maximum value for $\tau$, indicating that the optimum field from the fit is 3000 Oe. Again, fits including the Orbach contribution (see Figure S11, right, in the Supporting Information) gave $(\Delta E/k_B)_2 \approx 20$ K, far from that calculated using the $D$, $E$ ab initio parameters (~63 K). Therefore, the model based on the Raman-only contribution to the reversal of the magnetization displayed in eq 3 was also applied for modeling the $1/\tau$ vs $T$ data for **2**. The best fit is shown as a black solid line in the $1/\tau$ vs $T$ plot (Figure 7, bottom right), and yields $C = 7.03$ s$^{-1}$ K$^n$, $n = 5.10$. The variations in the $n$ values proposed by the fits for **1** (7.96) and **2** (5.10) may arise from the different orbital splitting of the d orbitals (see Theoretical Study) caused by differences in the crystal structure (vide supra). Those crystallographic dissimilarities might also influence the estimated Raman coefficients. Nevertheless, the values proposed for **1** and **2** are comparable to those for other reported Co-SIMs.

**Theoretical Study.** The zero-field splitting parameters in transition-metal complexes are determined by the zero-field splitting Hamiltonian[63−65]

$$\hat{H}_{ZFS} = D[\hat{S}_Z^2 - S(S+1)/3] + E(\hat{S}_X^2 - \hat{S}_Y^2) \quad (4)$$

where $D$ is the axial zero-field splitting (ZFS) parameter, $E$ is the rhombic ZFS parameter, and $S$, $S_X$, $S_Y$, and $S_Z$ are the total spin and its $x$, $y$, and $z$ components, respectively. By making the overall **D** tensor traceless, the three diagonal components are $D_{ZZ}$, $D_{YY}$, and $D_{XX}$ and the overall sign of $D$ can be determined by analyzing the sign of $D_{ZZ}$ since $D = 3/2\ D_{ZZ}$. The axial $D_{ZZ}$ term becomes dominant when the same $M_L$ level electronic transition takes place, which has been stated by us and others before.[66,67]

Both complexes possess an elongated tetrahedral geometry possessing pseudo-$D_{2d}$ symmetry. For complex **1**, the NEVPT2 method yields a $D$ value of −31.3 cm$^{-1}$ with $E/D$ estimated to be 0.11, while for complex **2** these are estimated to be $D = -21.9$ cm$^{-1}$ with $E/D = 0.08$ (Table 1). These values fit the magnetization data well, offering confidence in the estimated parameters. Earlier studies on tetrahedral Co$^{II}$ possessing $D_{2d}$ geometry suggest a large negative $D$ value for such geometries, as witnessed in the present case. The distortion from the $D_{2d}$ geometry particularly leads to a multideterminantal characteristic for the ground-state wave function with strong mixing


DOI: 10.1021/acs.inorgchem.8b01577
Inorg. Chem. 2018, 57, 13176−13187

with excited states as shown in Tables S5 and S6 in the Supporting Information with a major configuration possessing only 41% (62%) weighting to the ground-state wave function in complex **1** (**2**). This clearly suggests that the single-electron configuration cannot explain the given ligand field state, as observed also in other cases.[68] Between the two complexes, complex **2** is closer to $D_{2d}$ symmetry than **1**, leading to less mixing at the ground-state wave function. This is also reflected in the computed $E/D$ value, with complex **2** possessing a lower $E/D$ value in comparison to complex **1**. The computed eigenvalue plots for the d-based ligand field orbitals for complexes **1** and **2** are shown in Figure 8.

The origin of the negative $D$ parameter can be explained by the same $M_L$ level $d_{x^2-y^2} \rightarrow d_{xy}$ electronic transition taking place in both complexes, which is the first dominant electronic transition (see Tables S5−S8 in the Supporting Information). The gap between these two orbitals ($\Delta E$ of $d_{x^2-y^2}-d_{xy}$) increases from complex **1** to complex **2**. This can be explained from the increase of the torsional angle ($\theta_t$) from complex **1** (93 and 95°) to complex **2** (97 and 96°) (Figure S12 in the Supporting Information). A perfect $D_{2d}$ symmetry would lead to the $d_{z^2}$ orbital being lowest in energy followed by $d_{x^2-y^2}$ and $d_{xy}$ orbitals, where the maximum negative $D$ can be achieved.[69] The $D_{zz}$ and $g_{zz}$ axes (or the easy axes) in both complexes are along the pseudo-$C_2$ axis, as shown in Figure 9.

In both complexes the major structural parameters which control the zero-field splitting parameters are the O−Co−O bond angles (torsional angle mentioned by Vaidya et al.[70]) and the interplanar or dihedral angle (Table 2).[71] While $D$ is controlled by the first parameter, $E/D$ is controlled by the second parameter.

**Table 2. Selected Structural Parameters of Complexes 1 and 2 That Influence the Magnitude of $D$ and $E/D$**

| complex | dihedral angle ($\theta_d$) or interplanar angle (deg) | torsional angle ($\theta_t$, deg) | $D$ ($cm^{-1}$) | $E/D$ |
|---|---|---|---|---|
| **1** | 79.5 | O9−Co5−O3 = 92.75, O10−Co5−O4 = 95.38 | −31.31 | 0.11 |
| **2** | 82.1 | O9−Co5−O2 = 96.64, O8−Co5−O3 = 95.55 | −21.88 | 0.08 |

It has been observed that, as the O−Co−O angle ($\theta_t$) approaches 90°, the negative $D$ value increases. Therefore, complex **1** showing a higher negative $D$ value in comparison to complex **2** can be rationalized on the basis of this parameter. On the other hand, as the dihedral angle ($\theta_d$) deviates from 90°, the rhombic ZFS parameter ($E$ or $E/D$) increases. Consequently, the $E$ value is greater in complex **1** than in complex **2**.

All of our data suggest that symmetry plays a prominent role in controlling the sign of $D$, and our earlier studies on $\{CoS_4\}$[68] and $\{CoS_2X_2\}$[69] reveal the importance of donor atoms in switching the sign of the $D$ value, and here the $\{CoO_4\}$ unit is constrained in the presence of the diamagnetic $Co^{III}$ ions. This leads to a rather unusual distortion for the $\{CoO_4\}$ tetrahedra leading to negative $D$ values, which suggests the possibility of enhancing the single-ion $D$ value of mononuclear complexes by trapping them in certain diamagnetic environments.

As there are four $Co^{III}$ ions and one $Co^{II}$ ion, to understand if there is a valence delocalization present in these complexes, we have performed DFT calculations on complexes **1** and **2** using the Gaussian 09 suite of programs with the UB3LYP/TZV setup (see Computational Details). The computed spin density plots are shown in Figure 10 (Figure S13 in the Supporting Information). The $Co^{II}$ ion possesses a spin density of 2.742 and 2.734, respectively, for complexes **1** and **2**, revealing a localized picture of spin densities. The spin density on the $Co^{II}$ ions is slightly delocalized to the oxygen atom coordinated to the $Co^{II}$ ions (~0.05), while other atoms have very small contributions. In particular, all four $Co^{III}$ ions have negligible spin density, revealing primarily a valence-localized scenario, as revealed by the experiments and computed magnetic anisotropy.

## CONCLUSIONS

The synthetic marvel and role of the chosen ligand system established the power of direct reactions of the chosen Schiff base ligand system to grab five cobalt ions in two different oxidation states. The $[Co_5]$ coordination aggregates reported in this work represent a fascinating family of "*mixed-valent-mixed-geometry*" coordination of 3d ions. Growth of the structures for **1** and **2** rightly took place from spontaneous aggregation of two initially formed and highly reactive $\{Co^{III}_2(\mu\text{-L})(\mu\text{-OH/OMe})\}$ fragments through entrapment of a central $Co^{II}$ ion. This ion was responsible for providing significant magnetic anisotropy arising from the overall crystal

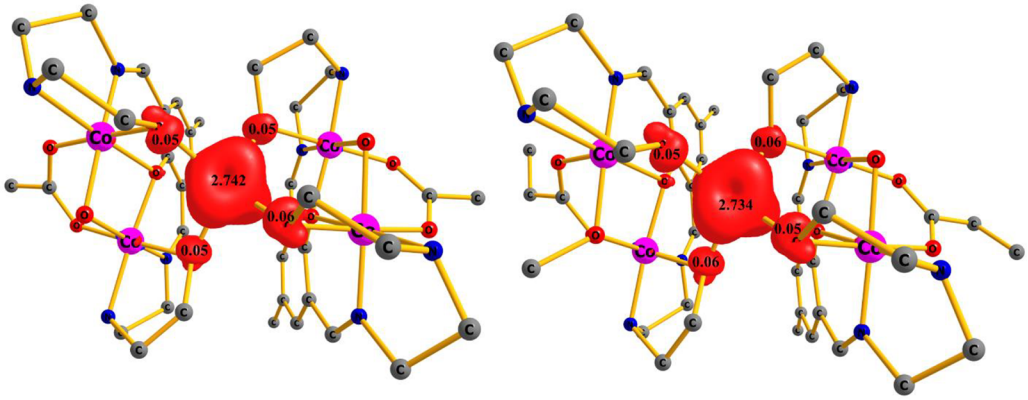


**Figure 10.** Spin density plots of complex **1** (left) and complex **2** (right). Color code: Co, pink;, O, red; N, blue; C, gray (hydrogen atoms are omitted for clarity). Spin densities are plotted using an isosurface value of 0.0065 e/bohr$^3$.



DOI: 10.1021/acs.inorgchem.8b01577
*Inorg. Chem.* 2018, 57, 13176−13187

field effects of the ligand system and several ancillary bridges. The experimental results were supported by theoretical calculations. The O−Co−O bond angles and the interplanar angles control the zero-field splitting parameters. The presence of two diamagnetic $\{Co_2(\mu\text{-L})\}$ hosts leads to a somewhat unusual distortion for the central $\{CoO_4\}$ tetrahedron in **1** and **2**, leading to negative *D* values. This observation highlights an opportunity for increasing the single-ion *D* value for pseudo-mononuclear $Co^{II}$ units by trapping them within a defined diamagnetic coordination environment.

## ■ ASSOCIATED CONTENT

### Supporting Information

The Supporting Information is available free of charge on the ACS Publications website at DOI: 10.1021/acs.inorgchem.8b01577.

Figures S1−S13 and Tables S1−S8 as described in the text (PDF)

### Accession Codes

CCDC 1534949−1534950 contain the supplementary crystallographic data for this paper. These data can be obtained free of charge via www.ccdc.cam.ac.uk/data_request/cif, or by emailing data_request@ccdc.cam.ac.uk, or by contacting The Cambridge Crystallographic Data Centre, 12 Union Road, Cambridge CB2 1EZ, UK; fax: +44 1223 336033.

## ■ AUTHOR INFORMATION


### Corresponding Authors

*E-mail for M.M.: Mark.Murrie@glasgow.ac.uk.
*E-mail for G.R.: rajaraman@chem.iitb.ac.in.
*E-mail for D.R.: dray@chem.iitkgp.ac.in.

### ORCID

Gopalan Rajaraman: 0000-0001-6133-3026
Debashis Ray: 0000-0002-4174-6445


### Notes

The authors declare no competing financial interest.

## ■ ACKNOWLEDGMENTS

K.C. is thankful to the Council of Scientific and Industrial Research, New Delhi, India, for financial support. We are also thankful to the DST, New Delhi, Indian, for providing the single-crystal X-ray diffractometer facility at the Department of Chemistry, IIT Kharagpur, under its FIST program. M.M. thanks the University of Glasgow for financial support. G.R. thanks the SERB for its financial support (EMR/2014/000247).

## ■ REFERENCES


(1) Canaj, A. B.; Nodaraki, L. E.; Ślepokura, K.; Siczek, M.; Tzimopoulos, D. I.; Lis, T.; Milios, C. J. A family of polynuclear cobalt complexes upon employment of an indeno-quinoxaline based oxime ligand. *RSC Adv.* **2014**, *4*, 23068−23077.

(2) Bera, M.; Curtiss, A. B.; Musie, G. T.; Powell, D. R. A new self-assembled $\mu_6$-sulfato hexanuclear cobalt(II) complex of a symmetric dinucleating ligand: Synthesis and X-ray structural analysis. *Inorg. Chem. Commun.* **2008**, *11*, 1033−1036.

(3) Stephenson, A.; Ward, M. D. Molecular squares, cubes and chains from self-assembly of bis-bidentate bridging ligands with transition metal dications. *Dalton Trans.* **2011**, *40*, 10360−10369.

(4) Modak, R.; Sikdar, Y.; Thuijs, A. E.; Christou, G.; Goswami, S. $Co^{II}_4$, $Co^{II}_7$, and a series of $Co^{II}_2Ln^{III}$ ($Ln^{III}$= $Nd^{III}$, $Sm^{III}$, $Gd^{III}$, $Tb^{III}$, $Dy^{III}$) Coordination clusters: Search for single molecule magnets. *Inorg. Chem.* **2016**, *55*, 10192−10202.

(5) Mondal, A. K.; Khatua, S.; Tomar, K.; Konar, S. Field-induced single-ion-magnetic behavior of octahedral $Co^{II}$ in a two-dimensional coordination polymer. *Eur. J. Inorg. Chem.* **2016**, *2016*, 3545−3552.

(6) Ferguson, A.; Parkin, A.; Sanchez-Benitez, J.; Kamenev, K.; Wernsdorfer, W.; Murrie, M. A mixed-valence $Co_7$ single-molecule magnet with $C_3$ symmetry. *Chem. Commun.* **2007**, *33*, 3473−3475.

(7) Sheikh, J. A.; Clearfield, A. Heterometallic $Co^{III}$−$Gd^{III}$ clusters as magnetic refrigerants. *Inorg. Chem.* **2016**, *55*, 8254−8256.

(8) Tang, X.; Ye, W.; Hua, J.; Chen, M.; Cheng, H.; Ma, Y.; Yuan, R. Four $Co^{II}$-$Gd^{III}$ mixed-metal phosphonate clusters as molecular magnetic refrigerants. *Inorg. Chim. Acta* **2016**, *453*, 142−148.

(9) Tong, J.; Demeshko, S.; John, M.; Dechert, S.; Meyer, F. Redox-induced single-molecule magnetism in mixed-valent [2× 2] $Co_4$ grid complexes. *Inorg. Chem.* **2016**, *55*, 4362−4372.

(10) Craig, G. A.; Murrie, M. 3d single-ion magnets. *Chem. Soc. Rev.* **2015**, *44*, 2135−2147.

(11) Liddle, S. T.; van Slageren, J. Improving f-element single molecule magnets. *Chem. Soc. Rev.* **2015**, *44*, 6655−6669.

(12) Zadrozny, J. M.; Long, J. R. Slow magnetic relaxation at zero field in the tetrahedral complex $[Co(SPh)_4]^{2-}$. *J. Am. Chem. Soc.* **2011**, *133*, 20732−20734.

(13) Frost, J. M.; Harriman, K. L. M.; Murugesu, M. The rise of 3-d single-ion magnets in molecular magnetism: towards materials from molecules? *Chem. Sci.* **2016**, *7*, 2470−2491.

(14) Meng, Y.-S.; Jiang, S.-D.; Wang, B.-W.; Gao, S. Understanding the magnetic anisotropy toward single-ion magnets. *Acc. Chem. Res.* **2016**, *49*, 2381−2389.

(15) Feng, M.; Tong, M.-L. Single ion magnets from 3d to 5f: Developments and strategies. *Chem. - Eur. J.* **2018**, *24*, 7574−7594.

(16) Zhu, Y. Y.; Cui, C.; Zhang, Y. Q.; Jia, J. H.; Guo, X.; Gao, C.; Qian, K.; Jiang, S.-D.; Wang, B.-W.; Wang, Z.-M.; Gao, S. Zero-field slow magnetic relaxation from single Co(II) ion: a transition metal single-molecule magnet with high anisotropy barrier. *Chem. Sci.* **2013**, *4*, 1802−1806.

(17) Mandal, D.; Ray, D. Self-assembly of a face-shared partial double cubane supported by alkoxo terminal and bridging ligands. *Inorg. Chem. Commun.* **2007**, *10*, 1202−1205.

(18) Sarkar, M.; Aromí, G.; Cano, J.; Bertolasi, V.; Ray, D. Double-$CO_3^{2-}$ centered $[Co^{II}_5]$ wheel and modeling of its magnetic properties. *Chem. - Eur. J.* **2010**, *16*, 13825−13833.

(19) Chattopadhyay, K.; Shaw, B. K.; Saha, S. K.; Ray, D. Unique trapping of paddlewheel copper(II) carboxylate by ligand-bound $\{Cu_2\}$ fragments for $[Cu_6]$ assembly. *Dalton Trans.* **2016**, *45*, 6928−6938.

(20) Chattopadhyay, K.; Craig, G. A.; Kundu, A.; Bertolasi, V.; Murrie, M.; Ray, D. Hydroxido-supported and carboxylato bridge-driven aggregation for discrete $[Ni_4]$ and interconnected $[Ni_2]_n$ complexes. *Inorg. Chem.* **2016**, *55*, 10783−10792.

(21) Gagne, R. R.; Spiro, C. L.; Smith, T. J.; Hamann, C. A.; Thies, W. R.; Shiemke, A. K. The synthesis, redox properties, and ligand binding of heterobinuclear transition-metal macrocyclic ligand complexes. Measurement of an apparent delocalization energy in a mixed-valent $Cu^ICu^{II}$ complex. *J. Am. Chem. Soc.* **1981**, *103*, 4073−4081.

(22) Neese, F. The ORCA program system. *Wiley Interdiscip. Rev. Comput. Mol. Sci.* **2012**, *2*, 73−78.

(23) Weigend, F.; Ahlrichs, R. Balanced basis sets of split valence, triple zeta valence and quadruple zeta valence quality for H to Rn: Design and assessment of accuracy. *Phys. Chem. Chem. Phys.* **2005**, *7*, 3297−3305.

(24) Hellweg, A.; Hattig, C.; Hofener, S.; Klopper, W. Optimized accurate auxiliary basis sets for RI-MP2 and RI-CC2 calculations for the atoms Rb to Rn. *Theor. Chem. Acc.* **2007**, *117*, 587−597.

(25) Maurice, R.; Bastardis, R.; Graaf, C. d.; Suaud, N.; Mallah, T.; Guihery, N. Universal theoretical approach to extract anisotropic spin Hamiltonians. *J. Chem. Theory Comput.* **2009**, *5*, 2977−2984.




DOI: 10.1021/acs.inorgchem.8b01577
*Inorg. Chem.* 2018, 57, 13176−13187

(26) Frisch, M. J.; Trucks, G. W.; Schlegel, H. B.; Scuseria, G. E.; Robb, M. A.; Cheeseman, J. R.; Scalmani, G.; Barone, V.; Petersson, G. A.; Nakatsuji, H.; Li, X.; Caricato, M.; Marenich, A.; Bloino, J.; Janesko, B. G.; Gomperts, R.; Mennucci, B.; Hratchian, H. P.; Ortiz, J. V.; Izmaylov, A. F.; Sonnenberg, J. L.; Williams-Young, D.; Ding, F.; Lipparini, F.; Egidi, F.; Goings, J.; Peng, B.; Petrone, A.; Henderson, T.; Ranasinghe, D.; Zakrzewski, V. G.; Gao, J.; Rega, N.; Zheng, G.; Liang, W.; Hada, M.; Ehara, M.; Toyota, K.; Fukuda, R.; Hasegawa, J.; Ishida, M.; Nakajima, T.; Honda, Y.; Kitao, O.; Nakai, H.; Vreven, T.; Throssell, K.; Montgomery, J. A., Jr.; Peralta, J. E.; Ogliaro, F.; Bearpark, M.; Heyd, J. J.; Brothers, E.; Kudin, K. N.; Staroverov, V. N.; Keith, T.; Kobayashi, R.; Normand, J.; Raghavachari, K.; Rendell, A.; Burant, J. C.; Iyengar, S. S.; Tomasi, J.; Cossi, M.; Millam, J. M.; Klene, M.; Adamo, C.; Cammi, R.; Ochterski, J. W.; Martin, R. L.; Morokuma, K.; Farkas, O.; Foresman, J. B.; Fox, D. J. *Gaussian 09, Revision A.02*; Gaussian, Inc., Wallingford, CT, 2016.
(27) *Smart and XPREP*; Siemens Analytical X-ray Instruments Inc., Madison, WI, 1995.
(28) Sheldrick, G. M. *SHELXS-97*; University of Göttingen, Göttingen, Germany, 1997.
(29) Sheldrick, G. M. Crystal structure refinement with *SHELXL*. *Acta Crystallogr., Sect. A: Found. Crystallogr.* **2008**, *64*, 112−122.
(30) Farrugia, L. *WinGX System, v. 1.80.05*;, University of Glasgow, Glasgow, U.K..
(31) Sheldrick, G. M. *SADABS: Software for Empirical Absorption Correction*; University of Göttingen, Institute fur Anorganische Chemie der Universitat, Göttingen, Germany, 1999−2003.
(32) *DIAMOND, Visual Crystal Structure Information System, version 3.1*; Crystal Impact, Bonn, Germany, 2004.
(33) Farrugia, L. J. *POV-Ray - 3.5*; University of Glasgow, Glasgow, U.K., 2003.
(34) Ferguson, A.; Parkin, A.; Murrie, M. Synthesis and structural characterisation of polynuclear cobalt complexes with partially-deprotonated Bis-tris. *Dalton Trans.* **2006**, 3627−3628.
(35) Maloth, S.; Kurapati, S. K.; Pal, S. Synthesis, structure, and properties of a pentanuclear cobalt(III) coordination cluster. *J. Coord. Chem.* **2015**, *68*, 1402−1411.
(36) Nakamoto, K. *Infrared and Raman Spectra of Inorganic and Coordination Compounds*, 4th ed.; Wiley: New York, 1986.
(37) Deacon, G. B.; Phillips, R. J. Relationships between the carbonoxygen stretching frequencies of carboxylato complexes and the type of carboxylate coordination. *Coord. Chem. Rev.* **1980**, *33*, 227−250.
(38) Konstantinović, S. S.; Radovanović, B. C.; Cakić, Ž.; Vasić, V. M. Synthesis and characterization of Co(II), Ni(II), Cu(II) and Zn(II) complexes with 3-salicylidenehydrazono-2-indolinone. *J. Serb. Chem. Soc.* **2003**, *68*, 641−647.
(39) Cotton, F. A.; Wilkinson, G. *Advanced Inorganic Chemistry*; Wiley: New York, 1989.
(40) Cotton, F. A.; Goodgame, D. M. L.; Goodgame, U. M. The electronic structures of tetrahedral cobalt(II) complexes. *J. Am. Chem. Soc.* **1961**, *83*, 4690−4699.
(41) Brader, M. L.; Kaarsholm, N. C.; Harnung, S. E.; Dunn, M. F. Ligand Perturbation Effects on a Pseudotetrahedral Co(II)(His) 3-ligand site- A magnetic circular dichroism study of the Co(II)-substituted insulin hexamer. *J. Biol. Chem.* **1997**, *272*, 1088−1094.
(42) Mahapatra, T. S.; Basak, D.; Chand, S.; Lengyel, J.; Shatruk, M.; Bertolasi, V.; Ray, D. Competitive coordination aggregation for V-shaped $[Co_3]$ and disc-like $[Co_7]$ complexes: synthesis, magnetic properties and catechol oxidase activity. *Dalton Trans.* **2016**, *45*, 13576−13589.
(43) Nesterov, D. S.; Chygorin, E. N.; Kokozay, V. N.; Bon, V. V.; Boča, R.; Kozlov, Y. N.; Shul'pina, L. S.; Jezierska, J.; Ozarowski, A.; Pombeiro, A. J. L.; Shul'pin, G. B. Heterometallic $Co^{III}_4Fe^{III}_2$ Schiff base complex: Structure, electron paramagnetic resonance, and alkane oxidation catalytic activity. *Inorg. Chem.* **2012**, *51*, 9110−9122.
(44) Yang, L.; Powell, D. R.; Houser, R. P. Structural variation in copper(I) complexes with pyridylmethylamide ligands: structural analysis with a new four-coordinate geometry index, $\tau_4$. *Dalton Trans.* **2007**, 955−964.
(45) Cirera, J.; Alemany, P.; Alvarez, S. Mapping the stereochemistry and symmetry of tetracoordinate transition-metal complexes. *Chem. - Eur. J.* **2004**, *10*, 190−207.
(46) Brown, I. D.; Altermatt, D. Bond-valence parameters obtained from a systematic analysis of the Inorganic Crystal Structure Database. *Acta Crystallogr., Sect. B: Struct. Sci.* **1985**, *41*, 244−247.
(47) Brown, I. D. Recent developments in the methods and applications of the bond valence model. *Chem. Rev.* **2009**, *109*, 6858−6919.
(48) Chilton, N. F.; Anderson, R. P.; Turner, L. D.; Soncini, A.; Murray, K. S. PHI: A powerful new program for the analysis of anisotropic monomeric and exchange-coupled polynuclear d- and f-block complexes. *J. Comput. Chem.* **2013**, *34*, 1164−1175.
(49) Zadrozny, J. M.; Telser, J.; Long, J. R. (2013). Slow magnetic relaxation in the tetrahedral cobalt(II) complexes $[Co(EPh)_4]^{2-}$ (E= O, S, Se). *Polyhedron* **2013**, *64*, 209−217.
(50) Fataftah, M. S.; Zadrozny, J. M.; Rogers, D. M.; Freedman, D. E. A mononuclear transition metal single-molecule magnet in a nuclear spin-free ligand environment. *Inorg. Chem.* **2014**, *53*, 10716−10721.
(51) Maganas, D.; Sottini, S.; Kyritsis, P.; Groenen, E. J. J.; Neese, F. Theoretical analysis of the spin hamiltonian parameters in $Co(II)S_4$ complexes, using density functional theory and correlated ab initio methods. *Inorg. Chem.* **2011**, *50*, 8741−8754.
(52) Carlin, R. L. *Magnetochemistry*; Springer-Verlag: Berlin, Heidelberg, 1986.
(53) Rechkemmer, Y.; Breitgoff, F. D.; van der Meer, M.; Atanasov, M.; Hakl, M.; Orlita, M.; Neugebauer, P.; Neese, F.; Sarkar, B.; van Slageren, J. A four-coordinate cobalt(II) single-ion magnet with coercivity and a very high energy barrier. *Nat. Commun.* **2016**, *7*, 10467.
(54) Herchel, R.; Váhovská, L.; Potočňák, I.; Trávníček, Z. Slow magnetic relaxation in octahedral cobalt(II) field-induced single-ion magnet with positive axial and large rhombic anisotropy. *Inorg. Chem.* **2014**, *53*, 5896−5898.
(55) Lunghi, A.; Totti, F.; Sanvito, S.; Sessoli, R. Intra-molecular origin of the spin-phonon coupling in slow-relaxing molecular magnets. *Chem. Sci.* **2017**, *8*, 6051−6059.
(56) Lunghi, A.; Totti, F.; Sessoli, R.; Sanvito, S. The role of anharmonic phonons in under-barrier spin relaxation of single molecule magnets. *Nat. Commun.* **2017**, *8*, 14620.
(57) Collet, A.; Craig, G. A.; Heras Ojea, M.; Bhaskaran, L.; Wilson, C.; Hill, S.; Murrie, M. Slow magnetic relaxation in a $\{Co^{II}Co^{III}_2\}$ complex containing a high magnetic anisotropy trigonal bipyramidal $Co^{II}$ centre. *Dalton Trans.* **2018**, *47*, 9237−9240.
(58) Walsh, J. P. S.; Bowling, G.; Ariciu, A.-M.; Jailani, N. F. M.; Chilton, N. F.; Waddell, P. G.; Collison, D.; Tuna, F.; Higham, L. J. Evidence of slow magnetic relaxation in $Co(AcO)_2(py)_2(H_2O)_2$. *Magnetochemistry* **2016**, *2*, 23.
(59) Pedersen, K. S.; Dreiser, J.; Weihe, H.; Sibille, R.; Johannesen, H. V.; Sørensen, M. A.; Nielsen, B. E.; Sigrist, M.; Mutka, H.; Rols, S.; Bendix, J. Design of single-molecule magnets: insufficiency of the anisotropy barrier as the sole criterion. *Inorg. Chem.* **2015**, *54*, 7600−7606.
(60) Abragam, A.; Bleaney, B. *Electron Paramagnetic Resonance of Transition Ions*; Oxford University Press, Oxford, 1970.
(61) Zhang, Y. Z.; Gómez-Coca, S.; Brown, A. J.; Saber, M. R.; Zhang, X.; Dunbar, K. R. Trigonal antiprismatic Co(II) single molecule magnets with large uniaxial anisotropies: importance of Raman and tunneling mechanisms. *Chem. Sci.* **2016**, *7*, 6519−6527.
(62) Novikov, V. V.; Pavlov, A. A.; Nelyubina, Y. V.; Boulon, M. E.; Varzatskii, O. A.; Voloshin, Y. Z.; Winpenny, R. E. A trigonal prismatic mononuclear cobalt (II) complex showing single-molecule magnet behavior. *J. Am. Chem. Soc.* **2015**, *137*, 9792−9795.
(63) Atanasov, M.; Aravena, D.; Suturina, E.; Bill, E.; Maganas, D.; Neese, F. First principles approach to the electronic structure, magnetic anisotropy and spin relaxation in mononuclear 3d-transition


DOI: 10.1021/acs.inorgchem.8b01577
*Inorg. Chem.* 2018, 57, 13176−13187

metal single molecule magnets. *Coord. Chem. Rev.* **2015**, *289-290*, 177−214.
(64) Rechkemmer, Y.; Breitgoff, F. D.; van der Meer, M.; Atanasov, M.; Hakl, M.; Orlita, M.; Neugebauer, P.; Neese, F.; Sarkar, B.; van Slageren, J. A four-coordinate cobalt(II) single-ion magnet with coercivity and a very high energy barrier. *Nat. Commun.* **2016**, *7*, 10467.
(65) Suturina, E. A.; Maganas, D.; Bill, E.; Atanasov, M.; Neese, F. Magneto-structural correlations in a series of pseudotetrahedral $[Co^{II}(XR)_4]^{2-}$ single molecule magnets: An ab initio ligand field study. *Inorg. Chem.* **2015**, *54*, 9948−9961.
(66) Gomez-Coca, S.; Cremades, E.; Aliaga-Alcalde, N.; Ruiz, E. (2013). Mononuclear single-molecule magnets: tailoring the magnetic anisotropy of first-row transition-metal complexes. *J. Am. Chem. Soc.* **2013**, *135*, 7010−7018.
(67) Ruamps, R.; Batchelor, L. J.; Maurice, R.; Gogoi, N.; Jiménez-Lozano, P.; Guihéry, N.; de Graaf, C.; Barra, A.-L.; Sutter, J.-P.; Mallah, T. Origin of the magnetic anisotropy in heptacoordinate $Ni^{II}$ and $Co^{II}$ Complexes. *Chem. - Eur. J.* **2013**, *19*, 950−956.
(68) Ruamps, R.; Batchelor, L. J.; Guillot, R.; Zakhia, G.; Barra, A.-L.; Wernsdorfer, W.; Guihéry, N.; Mallah, T. Ising-type magnetic anisotropy and single molecule magnet behaviour in mononuclear trigonal bipyramidal Co(II) complexes. *Chem. Sci.* **2014**, *5*, 3418−3424.
(69) Fataftah, M. S.; Coste, S. C.; Vlaisavljevich, B.; Zadrozny, J. M.; Freedman, D. E. Transformation of the coordination complex $[Co(C_3S_5)^{2]2-}$ from a molecular magnet to a potential qubit. *Chem. Sci.* **2016**, *7*, 6160−6166.
(70) Vaidya, S.; Upadhyay, A.; Singh, S. K.; Gupta, T.; Tewary, S.; Langley, S. K.; Walsh, J. P.; Murray, K. S.; Rajaraman, G.; Shanmugam, M. A synthetic strategy for switching the single ion anisotropy in tetrahedral Co(II) complexes. *Chem. Commun.* **2015**, *51*, 3739−3742.
(71) Vaidya, S.; Singh, S. K.; Shukla, P.; Ansari, K.; Rajaraman, G.; Shanmugam, M. Role of Halide Ions on the Nature of Magnetic Anisotropy in Tetrahedral $Co^{II}$ Complexes. *Chem. - Eur. J.* **2017**, *23*, 9546−9559.



DOI: 10.1021/acs.inorgchem.8b01577
*Inorg. Chem.* 2018, 57, 13176−13187